Available online at www.sciencedirect.com
ScienceDirect
Journal of Nuclear Materials 362 (2007) 215–221
journal of nuclear materials
www.elsevier.com/locate/jnucmat

Nuclear reaction analysis with ion microbeam of cross sections of surface layers deposited in a tokamak divertor

H. Bergsåker [a,*], B. Emmoth [b], P. Petersson [c], G. Possnert [c], J.P. Coad [d], J. Likonen [e], T. Renvall [e]

[a] *Division of Fusion Plasma Physics (Association EURATOM-VR), Alfvén Laboratory, School of Electrical Engineering, Royal Institute of Technology KTH, SE-10044 Stockholm, Sweden*
[b] *KTH MAP/ECS, Electrum 229, 164 40 Kista, Stockholm, Sweden*
[c] *Tandem Laboratory, Uppsala Universitet, Box 256, 751 05 Uppsala, Sweden*
[d] *Culham Science Centre, EURATOM/UKAEA-Fusion Association, Abingdon, Oxfordshire OX14 3DB, UK*
[e] *Association EURATOM-TEKES, VTT Processes, P.O. Box 1000, 02044 VTT, Espoo, Finland*

Abstract

Ion micro beam analysis has been applied to the investigation of plasma deposited layers covering the divertor tiles in the JET tokamak. Since the layers are about 100 μm thick they are too thick to be completely investigated by ordinary ion beam analysis. Cross sections of the layers were prepared by cutting and polishing. Elemental depth profiles were determined from the two dimensional images that could be derived by nuclear reaction analysis and resonant backscattering spectrometry, using ion beams focused to a few μm spot size. A combination of analysis methods are shown, which allow measurements of the concentration profiles of carbon, beryllium, deuterium, oxygen and stainless steel components at levels of a few percent, with an accuracy better than 10%.

PACS: 81.70.Jb; 52.40.Kh; 52.55.Fa

1. Introduction

A critical issue for the international thermonuclear experimental reactor (ITER) experiment and ultimately for a tokamak fusion reactor is the erosion and deposition at the surface of plasma facing materials. In particular if carbon is a major constituent of the plasma facing surfaces, the trapping of tritium fuel by co-deposition with carbon is of great concern. Moreover, if various materials are used in different plasma facing areas, there is a complicated problem of materials migration. In the JET experiment recently, most of the plasma facing surfaces have been made of a carbon fibre composite, while the vessel surfaces have been regularly conditioned by beryllium evaporation.

Ever since the build-up of thick deposited carbon layers and the associated co-deposition of hydrogen isotopes at plasma exposed surfaces in tokamaks

* Corresponding author. Tel.: +46 8 7906094; fax: +46 8 245431.
E-mail address: henric.bergsaker@alfvenlab.kth.se (H. Bergsåker).

0022-3115/$ - see front matter © 2007 Elsevier B.V. All rights reserved.
doi:10.1016/j.jnucmat.2007.01.046

was first discovered in JET [1–3], it has consequently been imperative to study the process. An obvious means to do so is to extract in-vessel components following periods of plasma operation and investigate the surfaces post mortem. The first depth profiles of deuterium in deposited layers in JET were measured by ion beam nuclear reaction analysis using the $^{2}H(^{3}He,p)^{4}He$ reaction with energy analysis of the protons [3]. This method and other direct ion beam analysis methods are most convenient for analysis up to a few microns depth. As the deposited layers in the fusion experiments grew thicker, up to hundreds of microns, other analysis methods had to be employed, which rely either on sectioning of the layers from the top or on cutting, breaking or polishing the samples in such a way that cross section of the deposited layer is presented for microscopy or spatially resolved analysis by various methods [4–8].

In this report investigations are presented of cross sections of deposited layers from JET using nuclear reaction analysis with an ion micro beam. It is shown that sufficient depth resolution and sensitivity can be achieved to study depth profiles of layers 50–100 μm thick. By mapping significant surface areas in this way, the actual surface composition during plasma operation can be monitored and net migration of material can be studied. In areas with continuous deposition the depth profiles may also permit the correlation in an archaeology manner of film composition with plasma operations parameters.

2. Experimental

The samples to be investigated were cut out from tiles which had been exposed to the plasma in the MkII GB gas box divertor 1999–2001 and in the MkII SRP divertor 2001–2004. Samples from tile 3 were in closer contact with the divertor plasma and subjected to erosion, mainly chemical sputtering, while samples from tile 4 come from a more remote area with only indirect contact with the plasma and less erosion. A recent review covers the conclusions so far about material re-deposition in the MkII-GB divertor and shows the geometry in the vessel and the distribution of tiles [9].

The samples were covered with an epoxy cladding and cut and polished so as to produce a surface presenting a cross section of the original deposited layer. Fig. 1 shows an optical micrograph of one of the deposited layers in cross section and defines

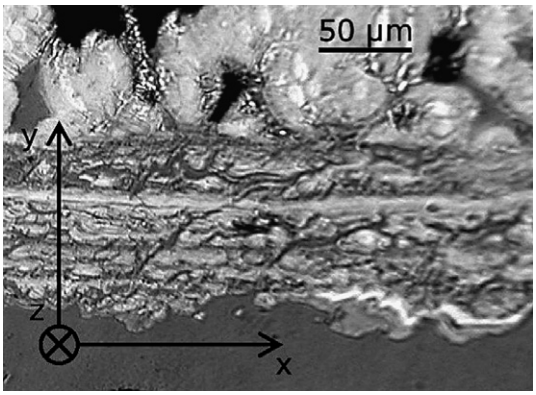

Fig. 1. Optical micrograph of a section of one of the samples (3/7a, exposed in the JET divertor 2001–2004). The original layer surface is in the *xz*-plane. The sample has been cut and polished perpendicularly to the original surface and analysis is performed across the *xy*-plane, with the analysing beam in the *z*-direction. The epoxy is found at the bottom, the CFC substrate at the top.

a coordinate system with the original tile surface in the *xz*-plane and the polished surface in the *xy*-plane. The analysed samples were about 15 mm wide in the *x*-direction.

The ion beam analysis facility is set up at the 5 MV tandem pelletron accelerator at the Ångström Laboratory in Uppsala. The microbeam line consists essentially of an adjustable rectangular aperture followed by a transport distance of about 6 m and a triplet quadrupole magnetic lens (Oxford Microbeams Ltd.) which focuses a reduced image of the aperture onto the sample [10]. The samples were oriented with the analysing beam in the *z*-direction and magnetic steering permits scanning in the *x*- and *y*-directions on the sample surface. Typically the beam was scanned stepwise over 512×512 pixels with 10 μs dwell time at each spot.

The control signals for the sweep were sampled in hardwired coincidence with any detected event in either of the two detectors which could be used simultaneously. By software coincidence conditions the *x*- and *y*-signals were sorted according to whether the particles were detected in any of a number of predefined energy regions. The data were also stored in list mode, so that both the energy of any detected particle and the corresponding beam position can be retrieved. An optical microscope and a *xy*-translation manipulator with 1.25 μm resolution were used to focus the beam and position the beam spot on the target. For spatial calibration the beam was scanned over Au or Cu grids of known dimensions and backscattered ions were used to determine the spatial calibration and spatial resolution. Fig. 2

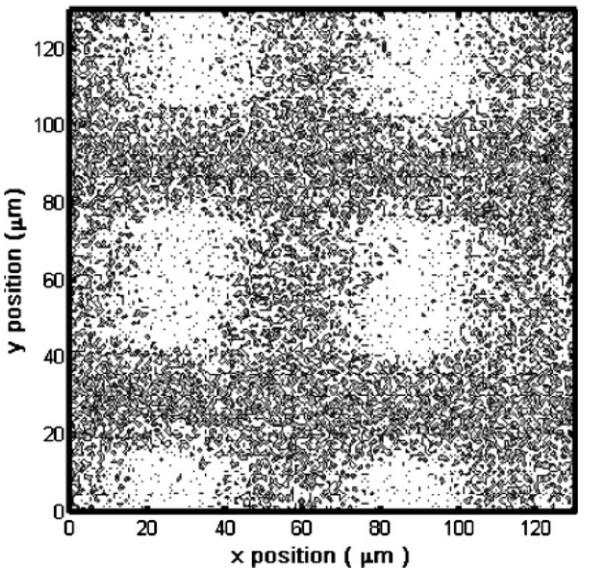

Fig. 2. A backscattering image of a square gold plated copper grid with a spatial period of 60 μm. The high energy part of the $^3He^+$ backscattering spectrum from the grid was selected for this plot. Before any measurement is performed, the spatial calibration and the spatial resolution are always determined by scanning a grid of known dimensions.

shows a backscattering yield image of a square gold plated Cu grid with 60 μm spatial period. The high energy part of the backscattering spectrum with 3 MeV $^3He^+$ beam has been selected. Fig. 3 shows the backscattering distributions projected onto the x- and y-axes, respectively, where the beam size can be determined from the edge sharpness. The solid lines show fits under the assumption that the current density distribution of the beam is Gaussian in both x- and y-direction:

$$j(x,y) = \frac{i}{2\pi\sigma_x\sigma_y} e^{x^2/2\sigma_x^2 + y^2/2\sigma_y^2}, \quad (1)$$

where i is the beam current and σ_x and σ_y standard deviations. For the x-direction, as shown in the upper part of Fig. 3 the best fit is for $\sigma_x = 10$ μm, while as shown in the lower part of the figure, in the y-direction $\sigma_y = 4$ μm gives the best fit. For the measurements presented below these conditions were typical, with $2 < \sigma_y < 5$ μm and $10 < \sigma_x < 20$ μm. With this beam size the achievable beam current was 50–150 pA.

For measuring the concentrations of carbon, deuterium and beryllium the $^{12}C(^3He,p)^{14}N$, $^2H(^3He,p)^4He$ and $^9Be(^3He,p)^{11}B$ nuclear reactions were used with 3.0 MeV $^3He^+$ beam. Protons were detected at $\theta = 131°$ interaction angle with a detector with 0.1 sr solid angle, 1500 μm depletion layer and covered with a 70 μm thick Al foil. The foil absorbs backscattered ^3He and low energy alpha particles, so that only protons and deuterons are detected. Spectra including backscattered ions were simultaneously recorded with a detector at $\theta = 135°$ and 4×10^{-2} sr solid angle. Fig. 4 shows an example of a proton spectrum from one of the samples.

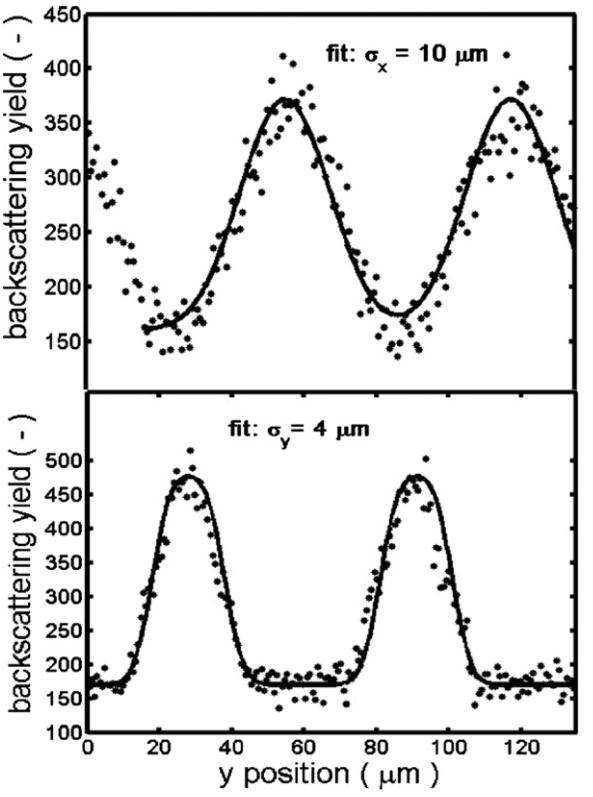

Fig. 3. Upper part: a projection of the grid pattern from Fig. 2 onto the x-axis. A spatial resolution $\sigma_x \approx 10$ μm can be determined. Lower part: the projection of the grid pattern from Fig. 2 onto the y-axis. A spatial resolution $\sigma_y \approx 4$ μm can be determined. This beam size is typical for the measurements discussed in this paper.

The absolute calibration was based on the proton yields from pure C and Be samples. It is assumed that the target composition is uniform throughout the accessible depth δz (less than 10 μm). The total proton yield from any of the tree nuclear reactions can then be written

$$Y_Z^M = c_Z \frac{Q}{e} \Omega \int_0^{E0} \frac{\sigma_Z(E)\mathrm{d}E}{\varepsilon^M(E)} = c_Z \frac{Q}{e} \Omega I_Z^M, \quad (2)$$

where Z represents the detected element, $\sigma_Z(E)$ is the differential reaction cross section at energy E, E_0 the incident ion energy, Q the collected charge, Ω

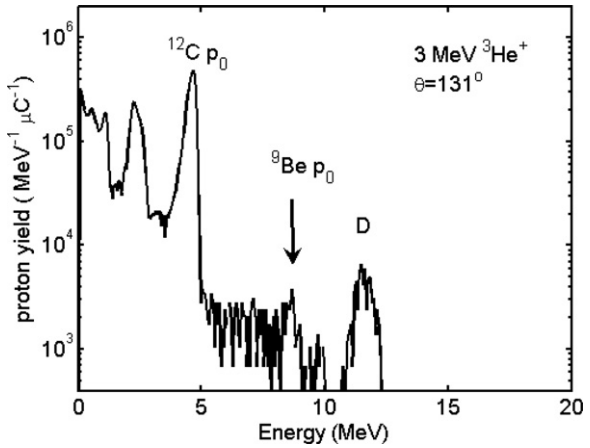

Fig. 4. An example of a proton spectrum, from sample 3/7a. The spectrum is averaged over the entire scanned area, including the cross section of the deposited layer, the CFC substrate and the epoxy cladding. The areas in the marked peaks are used for determining the concentrations of Be and D.

the solid angle, $\varepsilon^{M}(E)$ the ^{3}He stopping power in the matrix of composition M and c_Z the concentration of element Z with respect to matrix M, either elemental or a measured sample.The point in calibrating the measurement with pure samples is that the beryllium concentration can be derived from a spectrum like that in Fig. 4, irrespectively of $\sigma_C(E)$, $\sigma_{Be}(E)$, Q and Ω, provided that $\varepsilon^{C}(E)$, $\varepsilon^{Be}(E)$ and $\varepsilon^{M}(E)$ have nearly the same energy dependence over the energy range where the cross sections are significant.Since the results show that carbon is the main constituent in the layers and the oxygen concentration around 10%, it has been assumed for simplicity that the stopping power in the layers is everywhere approximately the Bragg stopping power of $CO_{0.1}$. Using stopping powers of Ref.[11], one finds that indeed the stopping power ratios $\varepsilon^{M}(E)/\varepsilon^{C}(E)$ and $\varepsilon^{M}(E)/\varepsilon^{Be}(E)$ change only by a few percent in the relevant energy range and the pure sample calibration measurement implies that the ratio of beryllium to carbon concentration can be calculated as $c_{Be}/c_Z = 1.28 \cdot Y^{M}_{Be}/Y^{M}_{C}$, where Y^{M}_{Be} and Y^{M}_{C} are the yields in the beryllium and carbon peaks shown in Fig. 4. In the case of deuterium, for lack of any stable calibration sample with known deuterium concentration, the bulk yield was calculated with Eq.(1), using the cross section fit from Ref. [12]. The integral of the cross section over the relevant energy range differs only by a few percent compared to the more recent measurement [13] and results in a deuterium to carbon ratio of $c_D/c_C = 0.051 \cdot Y^{M}_{D}/Y^{M}_{C}$, with Y^{M}_{D} being the yield in the deuterium peak of Fig. 4. These numbers were also compared with a simulation using SIMNRA [14] with cross sections from [13,15,16] and were found to agree within 6%. One concern when measuring deuterium with an ion beam analysis method is if deuterium is detrapped and released due to the ion beam. When this effect was investigated, less than 2% of the deuterium was found to be released during the analysis under the conditions described here.

Oxygen and medium Z constituents were measured by backscattering spectrometry with $^4He^+$, using an annular detector with 0.08 sr solid angle at $\theta = 170°$. The scattering resonance at 3.04 MeV [17,18] was used for increased sensitivity to oxygen and to be able to select the analysed volume for oxygen below the polished surface. The analysis was mostly run at 3.08 MeV, thus locating maximum sensitivity for oxygen at about 150 nm depth. Fig. 5 shows an example of a backscattering spectrum. The calibration for oxygen was made by comparison with a SiO_2 target and with the oxygen yield from the epoxy covering the analysed samples. The epoxy was found by RBS at 2 MeV to have an oxygen to carbon concentration ratio of about 11%. The two calibration methods agreed to within 10%. The whole area under the oxygen peak was used to calculate the oxygen concentration. As can be seen from Fig. 5 there is a background from heavier elements which should in principle be subtracted, since it differs between different positions on the target. Since this background is well below

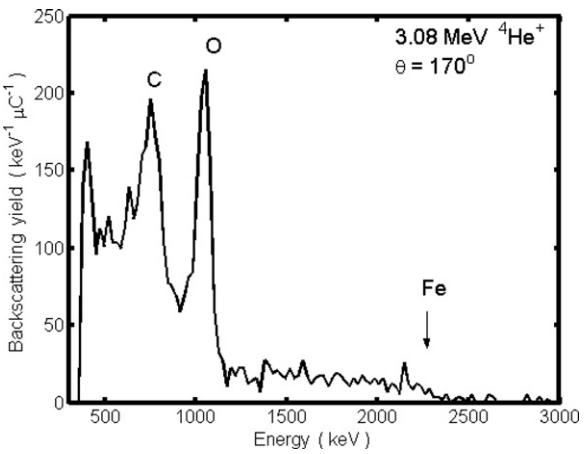

Fig. 5. An example of a backscattering spectrum. The resonant oxygen yield is used for determining the oxygen concentration. The part of the spectrum above 1.74 MeV is used for determination of the concentration of mainly stainless steel components. The spectrum is recorded from sample 3/7a at a fixed position at $y \approx 55$ μm from the original layer surface.

10% and does not change a lot, it was ignored. There are likely to be a couple of medium Z elements in the layers and they can not be clearly resolved by RBS. For simplicity the whole part of the spectrum corresponding to elements at the surface with $Z > 14$ was used as a rough measure of medium Z elements, and the concentration with respect to carbon was calculated assuming that they were mostly iron.

3. Results

Fig. 6 shows an example of two dimensional distributions of deuterium and beryllium in a layer cross section from tile 3, exposed to plasma 1999–2001. The mapping shows clearly that there is structure both in the x- and y-directions. Most notably, the deuterium concentration is relatively high near the original surface at $y = 0$, drops down between 20 and 40 μm below the surface and is again higher at larger depths. There is also some anti-correlation between deuterium and beryllium in that the deuterium depleted layer contains more beryllium Fig. 7 shows examples of depth profiles of deuterium, beryllium, oxygen and stainless steel components, which have been derived from mapping the cross section of a layer deposited on tile 3 during exposure

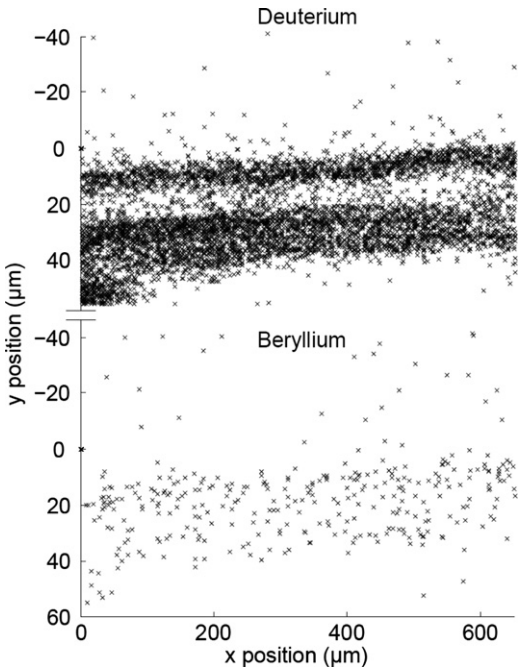

Fig. 6. Mapping of the 2d distributions of deuterium and beryllium for a cross section of the layer deposited on tile 3/1b, exposed 1999–2001.

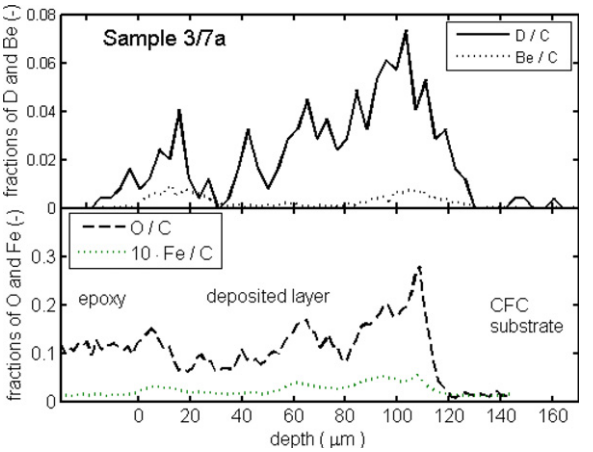

Fig. 7. Depth profiles of deuterium and beryllium (upper part), oxygen and stainless steel components (lower part) in sample 3/7a, exposed 2001–2004.

Table 1
Average thicknesses (measured with optical microscope) of the deposited layers and average concentrations of elements

Sample	3/1b	4/10a	3/7a
Exposure	1999–2001	1999–2001	2001–2004
Thickness (μm)	38 ± 6	65 ± 10	91 ± 25
O/C concentration ratio (%)	–	9	13
D/C concentration ratio (%)	2.1	25	0.3
Be/C concentration ratio (%)	1.6	–	3.3
Fe/C concentration ratio (%)	–	0.3	0.3

in 2001–2004. In this case, beryllium and deuterium are more correlated than in the older sample, reflecting different operations history. The oxygen content, reaching nearly 30% close to the layer-substrate interface, is clearly correlated with the stainless steel components, although the metal content is below 1%. Samples from tile 4, situated further away from the plasma, contained much more deuterium than those from tile 3 around 40% of the carbon concentration. This has already been observed with other methods. The results for the average concentrations of O, D, Be and medium Z elements are summarised in Table 1. Also shown in the table are the thicknesses of the layers measured with optical microscopy.

4. Discussion

The chosen reactions make it possible to analyse beryllium, deuterium, oxygen and stainless steel

components in carbon matrix, with reasonable accuracy down to a concentration level of one or a few atomic percent. The attraction with ion beam analysis compared e.g. to secondary ion mass spectroscopy is that the ion beam methods are easier to make completely quantitative. However, layers which are many tens of microns thick are not easily accessible to ion beam analysis from the surface. Making measurements along a surface cut perpendicular to the original one is then an attractive alternative, provided that the cutting and polishing procedure does not damage the concentration profiles or contaminate the new surface. As the layers are not uniform along the surface on the scale length of hundreds of μm or millimetres, some spatial resolution is necessary also in the direction along the original surface.

The spatial resolution in the present setup can be improved by reducing the size of the primary aperture, but there is a trade off with beam current and consequently with sensitivity and beam time requirement. For this work a compromise was chosen with a few microns resolution in the y-direction, where the strong concentration gradients appear, and typically 10–20 μm resolution in the perpendicular x-direction. As seen from Fig. 6, this choice is reasonable in view of the observed concentration gradients. The current density with this beam size is about 100 times higher than in normal conditions for ion beam analysis. The investigation shows that this is not a serious problem with respect to ion beam induced release of deuterium, if the beam is scanned. If the beam is left stationary on one spot during analysis however, the release of deuterium is substantial, up to half of the deuterium is then removed on the time scale of the measurement. The possibility to probe an analysed volume below the surface for oxygen analysis with the resonant backscattering technique is likely to be an attractive feature, preliminary results suggest that the oxygen concentration profiles are smeared out closer to the surface.

The present results show lower beryllium, deuterium and medium Z concentrations than earlier investigations [8,9]. Further investigations are needed to determine if this is due to differences in the methods or to the particular choices of samples. Qualitatively the results agree. The high deuterium concentration and low beryllium content in layers deposited in the more retracted area (tile 4) have for instance been shown before. The explanation is that carbon is eroded by chemical sputtering at the more exposed divertor surfaces and redeposited together with deuterium in the remote area. The electron temperature in the divertor is so low that hardly any physical sputtering occurs, leaving beryllium accumulated in the areas where carbon is eroded (tile 3) [8,9].

5. Conclusions

It has been shown that ion beam analysis with microprobe is a feasible option for investigating the layers several tens of microns thick which are deposited at plasma exposed surfaces in large tokamaks with carbon. The achieved spatial resolution and sensitivity is adequate for concentrations of Be, D, O and medium Z metals down to about 1%. The results are qualitatively in agreement with measurements by other methods.

Acknowledgements

This work has been supported by Vetenskapsrådet. The authors wish to thank A.P. Pisarev for fruitful discussions.

References

[1] G.M. McCracken, J. Ehrenberg, P.E. Stott, R. Behrisch, L. de Kock, J. Nucl. Mater. 145–147 (1987) 621.
[2] R. Behrisch, J. Ehrenberg, H. Bergsåker, J.P. Coad, L. de Kock, B. Emmoth, H. Kukral, G.M. McCracken, J.W. Partridge, J. Nucl. Mater. 145–147 (1987) 731.
[3] H. Bergsåker, R. Behrisch, J.P. Coad, J. Ehrenberg, B. Emmoth, S.K. Erents, G.M. McCracken, A.P. Martinelli, J.W. Partridge, J. Nucl. Mater. 145–147 (1987) 727.
[4] D.H.J. Goodall, G.M. McCracken, J.P. Coad, R.A. Causey, G. Sadler, O.N. Jarvis, J. Nucl. Mater. 162–164 (1989) 1059.
[5] D. Grambole, Fn. Herrmann, R. Klabes, W. Hauffe, R. Behrisch, Nucl. Instrum. and Meth. B 68 (1992) 154.
[6] R.D. Penzhorn, N. Bekris, J.P. Coad, L. Doff, M. Friedrisch, M. Gaugin, A. Haigh, R. Lasser, A. Peacock, Fus. Eng. Des. 49&50 (2000) 753.
[7] J. Likonen, S. Lehto, J.P. Coad, T. Renvall, T. Sajavaara, T. Ahlgren, D.E. Hole, G.F. Matthews, J. Keinonen, Fus. Eng. Des. 66–68 (2003) 219.
[8] J. Likonen, E. Vainonen-Ahlgren, J.P. Coad, R. Zilliacus, T. Renvall, D.E. Hole, M. Rubel, K. Arstila, G.F. Matthews, M. Stamp, J. Nucl. Mater. 337–339 (2005) 60.
[9] J.P. Coad, J. Likonen, M. Rubel, E. Vainonen-Ahlgren, D.E. Hole, T. Sajavaara, T. Renvall, G.F. Matthews, Nucl. Fus. 46 (2006) 350.
[10] F. Watt, G.W. Grime, Principles and Applications of High-Energy Ion Microbeams, IOP Publishing Ltd., Bristol, 1987.
[11] J.F. Ziegler, Helium Stopping Powers and Ranges in all Elemental Matter, Pergamon, 1977.
[12] C.J. Alstetter, R. Behrisch, J. Böttiger, F. Pohl, B.M.U. Scherzer, Nucl. Instrum. and Meth. 149 (1978) 59.

[13] V.Kh. Alimov, M. Mayer, J. Roth, Nucl. Instrum. and Meth. B 234 (2005) 169.
[14] M. Mayer, SIMNRA users guide, Report IPP 9/113, 1997.
[15] E.A. Wolicki, H.D. Holmgren, R.L. Johnston, E. Geer Illsey, Phys. Rev. 116 (1959) 1585.
[16] H. Kuan, T.W. Bonner, I.R. Risser, Nucl. Phys. 51 (1964) 481.
[17] J.R. Cameron, Phys. Rev. 90 (1953) 839.
[18] L.O. Norlin, B. Orre, G. Possnert, K. Johansson, Phys. Scr. 17 (1978) 439.